

pubs.acs.org/Biomac Article

Impact of Peptide Length and Solution Conditions on Tetrameric Coiled Coil Formation

Published as part of Biomacromolecules virtual special issue "Peptide Materials".

Joshua E. Meisenhelter, Nolan R. Petrich, Jacquelyn E. Blum, Albree R. Weisen, Rui Guo, Jeffery G. Saven,* Darrin J. Pochan,* and Christopher J. Kloxin*



Cite This: https://doi.org/10.1021/acs.biomac.4c00355



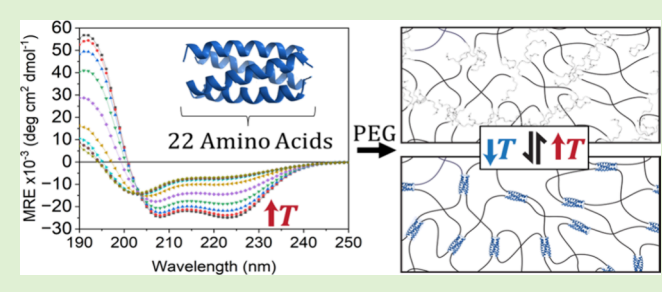
ACCESS

III Metrics & More

Article Recommendations

s Supporting Information

ABSTRACT: Unlike naturally derived peptides, computationally designed sequences offer programmed self-assembly and charge display. Herein, new tetrameric, coiled coil-forming peptides were computationally designed ranging from 8 to 29 amino acids in length. Experimental investigations revealed that only the sequences having three or more heptads (i.e., 21 or more amino acids) exhibited coiled coil behavior. The shortest stable coiled coil sequence had a melting temperature ($T_{\rm m}$) of approximately 58 \pm 1 °C, making it ideal for thermoreversible assembly over moderate temperatures. Effects of pH and monovalent salt were examined,



revealing structural stability over a pH range of 4 to 11 and an enhancement in $T_{\rm m}$ with the addition of salt. The incorporation of the coiled coil as a hydrogel cross-linker results in a thermally and mechanically reversible hydrogel. A subsequent demonstration of the hydrogel printed through a syringe illustrated one of many potential uses from 3D printing to injectable hydrogel drug delivery.

■ INTRODUCTION

Computational modeling allows for the prediction of peptide amino acid sequences that results in the formation of alpha helices and assembly into coiled coils, which can be viewed as monodisperse colloidal nanoparticles. 1,2 In nature, the coiled coil motif provides structural support to intricate proteins and enzymes, as illustrated in keratin proteins, which contain conserved coiled coils that form long rod-like structures.3 Additionally, coiled coils contribute dynamic properties to proteins as demonstrated in the influenza hemagglutinin protein, where coiled coils exhibit pH-responsive conformational changes, 4,5 or in the SNARE complex responsible for bringing cell membranes together. The synthetic coiled coil bundle unit, or bundlemer, acts similarly as a structural unit. Unlike its natural counterpart, bundlemers are computationally designed to be highly stable to various chemical variations at its exterior, allowing for extensive functionalization at specific locations on their periphery. For instance, the exterior of the bundlemer has been modified to be highly charged or present a programmed charge pattern, facilitating assembly into exotic 2D crystalline structures.² The well-defined structural and dynamic attributes of the bundlemer, combined with the potential for precise positioning of click chemical elements, yield an ideal building block capable of responding to environmental cues in a programmed manner.

Bundlemer-forming peptides are typically synthesized via automated solid-phase peptide synthesis (SPPS). The utilization of heated SPPS allows for rapid generation of both natural and non-natural sequences. For example, a typical 29 amino acid bundlemer-forming sequence is readily synthesized in less than 5 h. Reactive functional groups, such as click functionality, are incorporated to enable bundlemer cross-linking, resulting in extremely rigid-rod polymers. Incorporating coiled coils into other materials can result in a new material endowed with responsive attributes, such as dynamic hydrogels. The ability to swiftly prototype bundlemer-forming peptides with click-chemistry functionality and integrate them into bulk materials provides new avenues for advanced materials design.

One bundlemer-forming peptide sequence that has been recognized for its exceptional stability, particularly in response to modulation of exterior amino acid residues, is depicted in Figure 1 as BNDL29.² Generally, peptide sequences that form left-handed coiled coil assemblies follow a seven amino acid interaction repeat pattern or heptad.⁹ The BNDL29 sequence is constructed from four heptads with alanine (A), isoleucine (I), and methionine (M) in the first, fourth, and seven amino

Received: March 14, 2024 Revised: April 17, 2024 Accepted: April 18, 2024



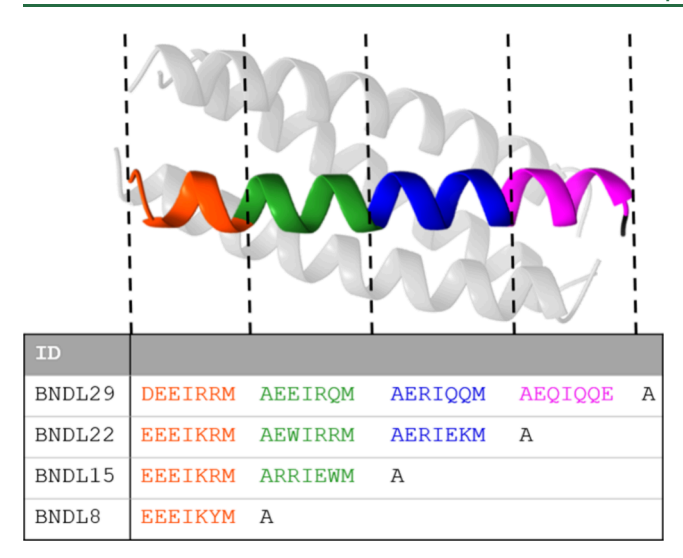


Figure 1. Rendering of an antiparallel tetrameric coiled coil (top) and the computationally optimized amino acid sequence predictions (bottom). Within the coiled coil, a single peptide helix is color-coded to illustrate the approximate positions of each heptad and their corresponding sequence, which is represented by their single letter amino acid code. Sequence written from the N- to C-terminus with the C-terminus containing an amide end-group.

acid positions of each heptad, respectively. This arrangement results in a peptide helix with a hydrophobic face consisting of alanine and isoleucine amino acids, making it amphiphilic and driving the formation of coiled coils within an aqueous environment. The computational design of BNDL29 ensures that four peptides assemble into a coiled coil, with the displayed exterior amino acids avoiding charge interactions that could lead to destabilization of the bundle, aggregation, or lattice formation.² Under pH-neutral conditions, BNDL29 exhibits excellent thermal stability, boasting a melting temperature in excess of 90 °C.¹ Moreover, the introduction of a wide range of designed mutations (i.e., substitutions) of amino acids at the exterior of the coiled coil with other polar and charged amino acids does not typically compromise its thermal stability, highlighting the robustness of the computational design.^{2,7,10}

The stability of a coiled coil is significantly influenced by the sequence length. For long coiled coil protein sequences (i.e., >10 heptads), stability is generally independent of chain length and dependent on properties like the positioning of hydrophobic residues within the sequence. 11 Conversely, for short coiled coil peptide sequences (i.e., <10 heptads), stability is highly dependent on chain length, where longer coiled coils are generally more stable. The minimum stable length for a dimeric coiled coil is usually 2-3 heptads based on observations from both natural and synthetic coiled coils. 12,13 Researchers have further enhanced the stability of short-length, 9-amino-acid helical peptides and coiled coil peptide assemblies through intra- and interhelical cross-links, respectively. 14,15 Additionally, the incorporation of salt bridging along the exterior of the coiled coil has been found to have drastically improved the stability of coiled coil peptides consisting of three heptads. 16 Shortening of peptide sequences is desirable from a practical viewpoint as synthetic yields increase and synthesis times decrease with decreasing peptide length. Moreover, shorter sequences are more sensitive to solution conditions, allowing for the dynamic tunability of materials

that incorporate bundlemers. Last, probing the lower bound of sequence lengths enhances our understanding of the fundamental principles associated with bundlemer design and engineering.

In this study, we explore coiled coil assembly as a function of peptide length by examining computationally designed peptides ranging from 1 to 4 heptads. We then focus on the shortest stable sequence and examine how salt, pH, and temperature affect its formation and stability. Last, drawing inspiration from the pioneering work of Tirrell and coworkers, we investigated the utilization of this computationally designed coiled coil within a hydrogel construct to impart a dynamic response to these otherwise inactive materials.

■ EXPERIMENTAL SECTION

Computational Design. Homotetrameric coiled coils were computationally designed using a previously described methodology.² Briefly, four heptad-based coiled coils were constructed using a mathematical model of a helix, which was parametrized by the superhelical radius, superhelical phase, relative displacement of the ends along the superhelical axis, minor helical phase, and superhelical pitch. These parameters were varied based on observations from natural coiled coil structures. 17,18 The mathematical coiled coil description was then constructed by invoking D_2 symmetry (Figure 2a). The probabilities of the hydrophobic amino acids (i.e., A, V, I, L, M, F, Y, and W) residing in the interior were assessed using statistical theory, enabling the calculation of internal energy.^{2,7} Monte Carlosimulated annealing over the structural parameters was used to identify local energy minima, guiding the selection of A, I, and M for the first, fourth, and seventh amino acid positions, respectively, in the heptad repeat.² In prior work, the amino acids that reside at the exterior were evaluated using this statistical design approach while also selecting directional self-complementary interactions to form specific coiled coil-based crystalline lattices. A nonlattice forming sequence 19 was identified as a control in that work. Here, we utilized this base sequence, designated as BNDL29, and applied the same statistical design approach to shorter sequences.

Newly optimized sequences were generated that contained 22, 15, and 8 amino acids, corresponding to 3, 2, and 1 heptads, respectively, based on BNDL29 as a reference (see Figure 1). The antiparallel nature of BNDL29 implies that simply truncating the sequence to achieve length variations would likely lead to misalignment of exterior residues (Figure 2b). The initial backbone design of BNDL29 followed a de novo approach.² The backbone featuring a densely packed hydrophobic interior core was selected. While shorter sequences may not be expected to form helical coiled coils, to maintain hydrophobic packing and consistency in the design, the backbones of the BNDL8, BNDL15, and BNDL22 variants (shown in Figure 1) were created using the same set of helical parameters as BNDL29.²

For the BNDL8, BNDL15, and BNDL22 variants, amino acid identities at hydrophobic positions mirrored those of BNDL29 (i.e., A, I, and M in the first, fourth, and seventh heptad positions, respectively) to preserve the integrity of the hydrophobic core (Figure 2c,d). The identities of exterior residues were determined using the same probabilistic approach used to calculate BNDL29; this involved calculating the probabilities of amino acids at each site to guide the sequence selection. Once the most probable amino acid along the exterior was identified, it was fixed, and the calculations were repeated until all of the amino acids residing at the exterior were determined. The exterior sites for BNDL8, BNDL15, and BNDL22 allowed for 18 types of natural amino acids (excluding proline and cysteine). To enable accurate concentration characterization via UV-vis spectroscopy, the location of a tryptophan (W) or tyrosine (Y) was initially identified based on the probability profiles (Y at position 6 in BNDL8, W at position 13 in BNDL15, and W at position 10 in BNDL22). The tryptophan or tyrosine was kept constant in subsequent calculations, with the most probable amino acid type selected for the remaining

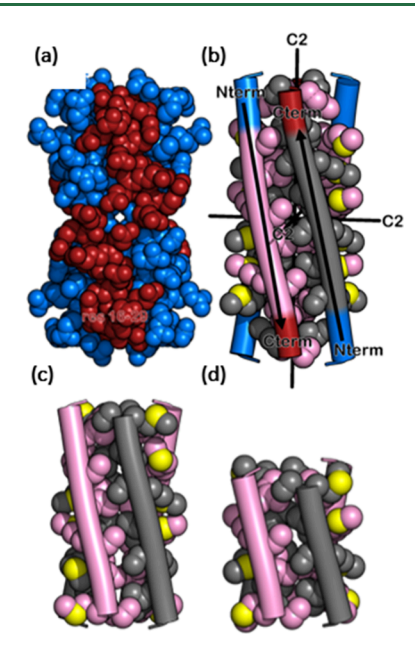


Figure 2. BNDL29, BNDL22, and BNDL15 models. (a) Space filling model of the BNDL29 peptide. Residues 1-15 are colored in blue, and residues 16-29 are colored in red. The blue-end residues interact with the red-end residues from the antiparallel neighboring helix, making the simple truncation of the sequence not optimal for creating shorter bundles. (b) Rendering of the antiparallel and D₂ features in BNDL29. Each helical backbone is represented by a cylinder, and the N-termini are colored in blue and C-termini in red. Antiparallel helices aligning in opposite directions are colored differently, chains in the top \rightarrow bottom direction (N \rightarrow C terminus) are colored in pink, and the neighboring antiparallel helices are colored in gray. The three C₂ rotation axes inherent to the D₂ symmetry are drawn. The hydrophobic interior core is rendered as spheres, where the carbon atoms adopt the same pink/gray color scheme as the cylinder models. (c, d) The backbone structures of BNDL22 and BNDL15 are built using the same Crick's parameters as BNDL29, and the interior residues (rendered in spheres) were kept, preserving the hydrophobic core. The pink/gray coloring scheme for antiparallel chains is the same as panel (2b).

exterior residues. Another synthetic consideration was the substitution of aspartic acid with glutamic acid to prevent the possible formation of aspartimide during synthesis. 20

Peptide Synthesis and Characterization. All chemicals and reagents were obtained from Fisher Scientific, unless otherwise stated. The designed sequences were synthesized via microwave-assisted solid-phase peptide synthesis (SPPS) following standard Fmocdeprotection protocols.²¹ Synthesis was performed on Rink-amide resin (ChemPep) with Fmoc-amino acids (ChemPep) being doublecoupled using diisopropylcarbodiimide (TCI) and OxymaPure (CEM) in 8 and 4 times excess, respectively, in dimethylformamide. This approach utilized microwave-assisted heating (Liberty Blue, CEM) to rapidly reach coupling temperatures of 90 °C, allowing for 2 min coupling times. After each coupling, the Fmoc protecting group was removed with a single deprotection using 20 v/v% piperidine (Sigma-Aldrich) in dimethylformamide at 75 °C for 3 min. After synthesis, the peptide was cleaved from resin using a trifluoroacetic acid (TFA) cleavage cocktail (92.5/2.5/5 v/v% TFA (Honeywell)/ water/triisopropylsilane (Chem Impex) with 50 mg/mL phenol (TCI) and 50 mg/mL 1,4-dithiothreitol (Chem Impex)) for 3 h. The crude product was precipitated by using ice-cold diethyl ether. The precipitate was isolated via centrifugation at 3000 relative centrifugal force (rcf) (Eppendorf centrifuge 5702R) for 6 min at 4 °C, followed by decanting of the ether. The pellet was washed three times by resuspending it in fresh ether, centrifuging, and isolating the solid peptide each time. Finally, the peptide pellet was dried under a stream

of nitrogen overnight, yielding a solid crude peptide. The resulting solid was redissolved in water and purified using reverse-phase high-performance liquid chromatography (HPLC) (Waters 2535). A gradient from 5 to 95% acetonitrile in water with 0.4% TFA was used to purify the peptides. The molecular weights of the peptides were confirmed via ultraperformance liquid chromatography—mass spectroscopy (LC-MS) (Xevo G2-XS QTof, Waters) (Figure S1), and the fractions containing the purified product were lyophilized (Labconoco, FreeZone) to a solid powder.

In preliminary work, it was observed that residual TFA from the synthesis and purification process impacted the consistency of the results: specifically, the determination of the melting temperatures and the propensity to aggregate (Figure S16). To address this issue, a method adapted from Ford and Kloxin was used to remove TFA from the peptide product. ²² Briefly, TFA was removed by dissolving the peptide product in water at a concentration of 1 mg/mL and adjusting the pH of the solution to 4 via the addition of hydrochloric acid (HCl). The peptide solution was then placed in 1 kDa dialysis tubing (G-biosciences, tube-O-DIALYZER) and dialyzed against acidified water (pH 4). The acidified water was replaced every 4 h over a 24 h period to displace any TFA salts bound to the peptide. After 24 h, the sample was dialyzed against non-pH-adjusted deionized (DI) water, with the water being replaced every 4 h over another 24 h period to remove residual HCl. The removal of TFA was confirmed via F¹⁹ NMR (Neo 400 MHz, Bruker) via the disappearance of the peak at -76 ppm.

The peptides' secondary structure was assessed using circular dichroism spectroscopy (CD) (Jasco-1500). Solid peptide samples were gravimetrically weighed and dissolved in water to the required concentration, which was confirmed using UV-vis spectroscopy (Thermo Scientific Nanodrop 2000C) at 280 nm. Samples were heated from 10 to 90 °C at a rate of 1 °C/min, and CD spectra were collected in 10 °C increments. CD spectra were obtained with a 1 mm path length quartz cuvette over a range of 185-250 nm with a digital integration time (D.I.T.) of 4 s, a scanning speed of 50 nm/min, and averaging 3 accumulations. The melting temperature (T_m) was determined by identifying the inflection point in the CD absorption at 222 nm as a function of temperature, reported in Table 1. The inflection point was determined by fitting the collected values at 222 nm with a Boltzmann sigmoidal curve using a Levenberg-Marquardt iteration algorithm in Origin software. The CD data were reported as concentration-corrected mean residue ellipticity (MRE), where MRE = CD/ $(l \cdot c \cdot n)$ and CD is the ellipticity, l is the path length, c is the peptide concentration, and n is the number of amino acid residues in the peptide.23

The impact of salt and pH on the thermal stability of the coiled coil was investigated using thermal sweeps in CD. Samples were prepared with the BNDL22 sequence at a peptide concentration of 0.1 mM, as determined by UV—vis spectroscopy. To investigate the effect of monovalent salt on coiled coil formation, a peptide solution with NaCl, NaF, KCl, or KF at a salt concentration of 20, 70, or 120 mM was prepared in deionized (DI) water without pH adjustment, yielding a pH of approximately 5. Additionally, the influence of pH on coiled coil formation was investigated by initially dissolving the peptide in DI water, yielding a pH of approximately 5, and then adjusting the pH lower or higher by adding HCl or NaOH, respectively, as determined by a pH probe (Thermo Scientific, OrionStar A215 & Orion ROSS Sure-Flow Semi Micro probe).

Hydrogel Formation and Characterization. Dynamic hydrogels were formed via a radical-mediated thiol—ene reaction between alkene-functionalized BNDL22 and a tetrafunctional poly(ethylene glycol) (PEG)-thiol star polymer. The alkene-functionalized BNDL22 was synthesized by incorporating an alkene-functionalized lysine at the N-terminus of the peptide sequence, which, once assembled, results in a tetrafunctional alkene coiled coil. Specifically, a lysine with an N-epsilon alloxycarbonyl (alloc) protecting group (Chem Pep) was used as an alkene-functional handle. The alloc protecting group is resistant to TFA deprotection and remains after cleavage from the resin. Following peptide purification, the resulting product was obtained as a solid powder. The peptide was dissolved in water to

form a coiled coil, which was confirmed through CD spectroscopy. To the peptide solution, a 20 kDa tetrafunctional PEG-thiol (JenKem) and the lithium phenyl-2,4,6-trimethylbenzoylphosphinate (LAP) photoinitiator were added (10 mM BNDL22, 11 mM LAP, and 2.5 mM PEG-4SH) and equilibrated to 50 $^{\circ}$ C.

Hydrogel formation was assessed in real time by monitoring the elastic and viscous moduli as a function of time using parallel-plate photorheometry (HR30, TA Instruments), which irradiates the specimen through the bottom plate (see Figure S15 for a typical plot of moduli versus time of irradiation). An 8 mm sandblasted parallel plate was chosen as the upper plate geometry to avoid slip of hydrogels. Each hydrogel was prepared by loading the liquid reactants onto the rheometer and irradiating the specimen with 365 nm light (OmniCure Series 2000, Excelitas Technologies) at an intensity of 20 mW/cm² for 3 min, enabling real-time property measurement and confirmation of gelation. The properties of resulting hydrogel were further characterized using oscillatory shear rheology as a function of temperature and strain, maintaining a fixed gap of 300 μ m.

Isothermal strain cycling experiments were performed at 22 °C with a fixed frequency of 1 Hz (6.28 rad/s) ranging from 1 to 600% strain. Isostrain holds were carried out at both high strain (600%) and low strain (1%) for 30 s each. A total of 4 strain cycles were performed on the hydrogels to determine the mechanical recoverability of the BNDL22 cross-linked hydrogels.

Isothermal holds were performed at 22 $^{\circ}$ C for 2 min at 5% strain and 1 Hz, with a temperature set-point equilibration time of 20 s. Following the 2 min sweep at 22 $^{\circ}$ C, the set temperature was immediately changed to 60 $^{\circ}$ C and allowed to equilibrate for 20 s. Upon reaching equilibration at 60 $^{\circ}$ C, another 2 min sweep at 5% strain and 1 Hz was carried out. Temperature cycling between 22 and 60 $^{\circ}$ C was completed over 4 cycles to assess the temperature-dependent mechanical recovery of the BNDL22 cross-linked hydrogels.

RESULTS AND DISCUSSION

Peptide Synthesis and Characterization. The secondary structures of the coiled coil-forming peptides were assessed by using CD spectroscopy, as shown in Figure 3. The CD spectra of BNDL29 and BNDL22 at 20 °C exhibit minima at 208 and 222 nm and a maximum at ~190 nm, which are characteristic of helical structure.²⁵ Examining the ratio of 222 nm to 208 nm for BNDL29 and BNDL22 shows a value of \sim 1, indicating the presence of coiled coils rather than α -helices. ^{13,26} The temperature dependence of the secondary structure of the BNDL22 peptides was investigated by increasing the temperature from 10 to 90 °C while monitoring the CD spectra, as shown in Figure 3. As previously reported, BNDL29 exhibits $T_{\rm m} > 90~^{\circ}{\rm C}$ at a pH of approximately 5 in DI water. BNDL22 exhibits a $T_{\rm m}$ of 58 \pm 1 °C, with complete disassociation to random coils at temperatures above approximately 70 °C (see Figure S6A). Conversely, the CD spectra of BNDL15 and BNDL8 at 20 °C only exhibited a minimum around 200 nm, indicating random-coil structures (see Figures S2B and S3B, respectively).²⁷ Additionally, there was no discernible change in secondary structure across a peptide concentration ranging from 200 to 6.25 µM (Figure

While computational design predicts sequences for a given coiled coil structure, previous observations indicated that such short sequences were unlikely to form experimentally. Specifically, 2-heptad long peptide sequences, without the addition of covalent linkages or copious salt bridging, are generally not observed to form coiled coils in nature. A requirement of at least 3 heptads for coiled coil formation has been demonstrated for various dimeric coiled coils. Studies by Fairman et al. Suggested that the impact of peptide length

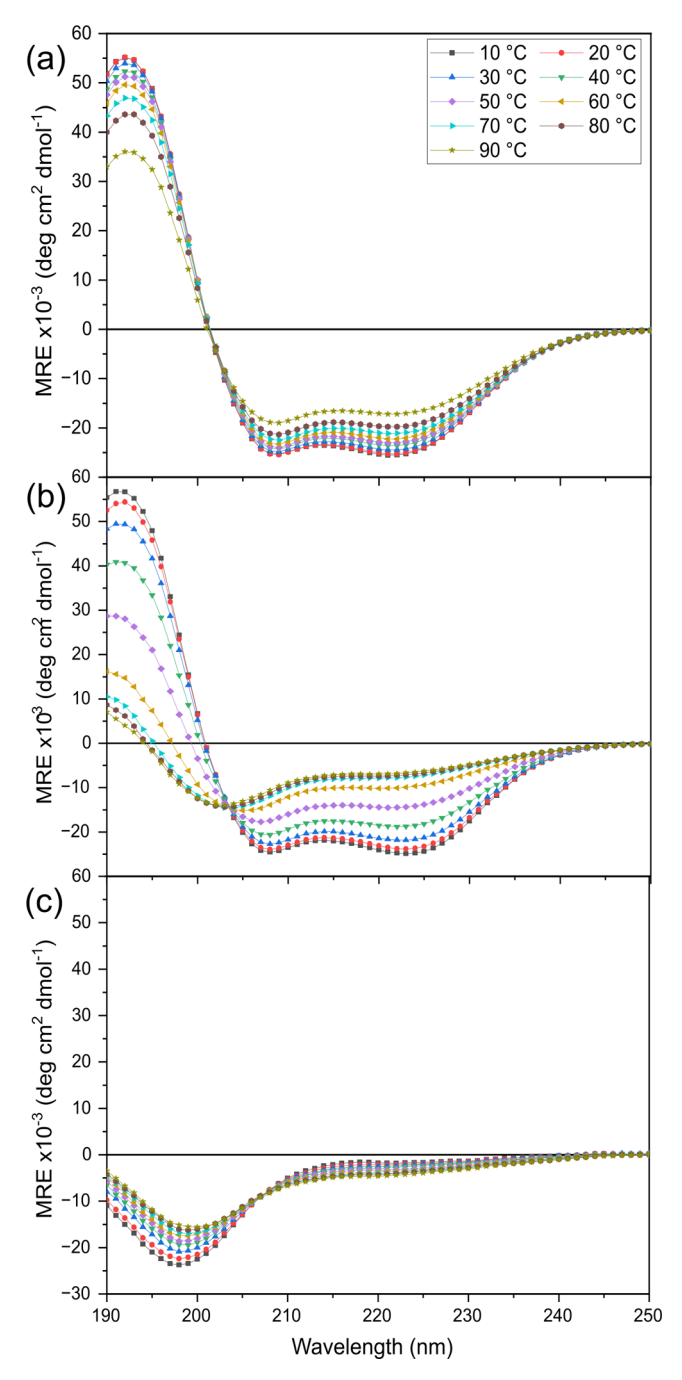


Figure 3. CD spectra for BNDL29, BNDL22, and BNDL15 peptides at a concentration of 100 μ M, plotted as mean residue ellipticity (MRE) versus wavelength. CD spectra of (a) BNDL29, (b) BNDL22, and (c) BNDL15 show the secondary structure of the peptide at 100 μ M in DI water without pH adjustment, resulting in a pH of ~5. CD spectra of BNDL8 (Figure S2B) is analogous to BNDL15. BNDL29 and BNDL22 peptides exhibited coiled coil formation, indicated by a maximum at 195 nm and minima at 208 and 222 nm, with the 222 nm/208 nm ratio of approximately 1. The BNDL15 sequence displayed a random coil structure due to the minimum at 200 nm. This suggests that BNDL15, consisting of 2 heptads, is too short to form a stable coiled coil. All samples were measured at 20 °C in DI water without pH adjustment, resulting in a pH of ~5.

is more significant in tetramers compared to dimers. This effect is attributed to the increased change in free energy per heptad in tetramers, which was attributed to the increased burial of hydrophobic residues. 28 The stability constraint of \geq 3 heptads

has been hypothesized to be due to a lack of favorable interactions within short coiled coil sequences; ¹⁵ thus, despite the higher degree of contact in tetrameric compared to dimeric coiled coils, we observe a similar length limitation in computationally designed tetramers optimized for stability. Consistent with these findings, we found that BNDL22 is the smallest peptide in this series capable of forming a stable coiled coil, making it suitable for material applications without additional external stabilization.

Impact of Solution Conditions on Stability. The presence of salt can have either a stabilizing or destabilizing effect on the coiled coil structure based on the amount and type of salt. Salt can screen both intracoiled coil charge interactions of amino acids along the exterior and intercoiled coil charge interactions of amino acids between coiled coils. Moreover, the type of salt present can significantly affect the coiled coil stability. Many salts have been categorized into what is known as the Hoffmeister series, which orders salts based on their observed propensity to promote or disrupt interactions, leading to either a "salting in" or "salting out" effect on proteins and peptides.^{29,30} "Salting in" refers to the solubilization of a protein in the presence of salt, while "salting out" describes the precipitation of a protein caused by the preferential interaction of some salts with water or the protein surface.³¹ Considering the influence of salt on proteins, it might be expected that monovalent salts such as KCl would enhance the stability of coiled coils. This increased stability has been explained as an increased hydrophobic effect, where in the presence of the salt, water is available to preferentially interact with amino acid side chains.32

Table 1. Melting Temperatures of BNDL22 at 0.1 mM in Different Monovalent Salt Solutions at 100 mM

salt	$T_{\rm m} \pm 1 (^{\circ}{\rm C})$
no salt	58
NaCl	69
KF	86
NaF	80
KCl	71

Solutions of BNDL22 were prepared over a range of salt types and concentrations in DI water without pH adjustment, yielding a pH of approximately 5, and their CD spectra were recorded as a function of temperature to explore the effects of solution salinity on the coiled coil secondary structure. Salts with multivalent ions, specifically magnesium sulfate and sodium citrate, were found to cause precipitation of BNDL22, which is also observed in various other protein systems. 33,34 To focus on the effects of different salt anions and cations, monovalent salts, specifically NaCl, NaF, KCl, and KF, were selected. In all cases, the addition of these salts resulted in an increase in melting temperature, with an increase in $T_{\rm m}$ as the salt concentration was increased up to 120 mM (Figures S8-S11). The increase in the thermal stability is consistent with the screening of unfavorable charge interactions along the exterior of the coiled coil. Notably, F had a greater stabilizing effect than Cl⁻, and K⁺ had a greater stabilizing effect than Na⁺, as evidenced by the increases in $T_{\rm m}$ (see Table 1). These trends align with the increases in protein stability described by the Hoffmeister series, resulting from the enhanced stabilization of the hydrophobic core responsible for the self-assembly of the coiled coil. 35,36

The protonation state of charged side groups is determined by their individual pK_a values, impacting the overall charge of the coiled coil in response to pH changes. Studies, such as that of Dutta et al., typically focus on pH solution conditions between 5.5 and 8.5, owing to the pK_a of the basic and acidic amino acid side groups;³⁷ furthermore, many of these studies have observed enhanced coiled coil stability within an acidic pH range of 6.5 to 2.³⁸ This finding may seem counterintuitive, particularly for dimeric coiled coils reliant on salt bridging interactions to maintain their structure, such as those associated with lysine-glutamic acid.³⁸ Importantly, it has been demonstrated that the influence of pH on stability is contingent upon the ionic strength. This relationship between ionic strength and pH trends was elucidated in a dimeric coiled coil system, where, at 100 mM NaCl, there was a shift to increased stability under acidic conditions.³⁸ As discussed in the context of the Hoffmeister series, the influence of salt on coiled coil stability is consistently observed; additionally, there is an intrinsic correlation between salt and pH. Salt aids in stabilizing the coiled coil at high pH by screening like-charge interactions. Conversely, at low pH, salt destabilized the coiled coil due to acidic side chains becoming partially protonated and thus no longer charged.³⁷

The impact of pH on the stability of BNDL22 was investigated by adjusting the pH. Given that sodium and chloride ions predictably affect stability, we selected HCl or NaOH to adjust the pH from 2 to 13 of the BNDL22 solutions, as shown in Figure 4. The transition from coiled coils to unfolded random coils was assessed by monitoring the ratio of ellipticities at 222 nm and the isodichroic point at 204 nm. This metric was selected because the ellipticity at 222 nm

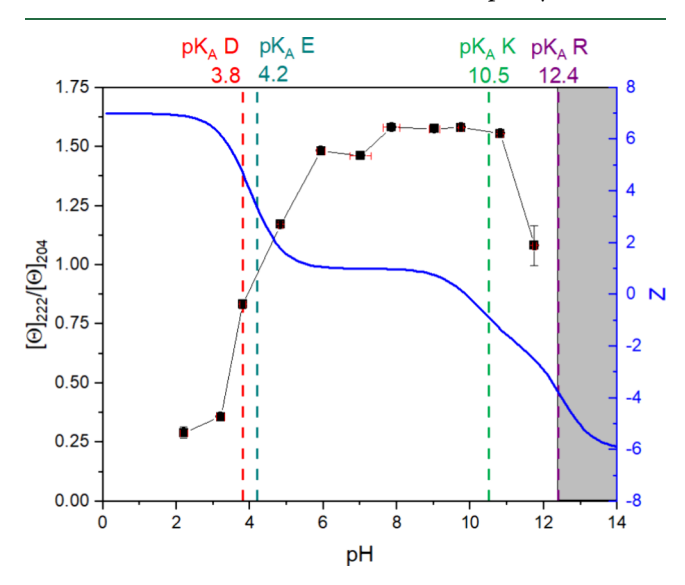


Figure 4. Effect of pH on the stability of the BNDL22 coiled coil structure. The ratio of 222 nm to 204 nm, as measured via CD, was used as an indicator for the presence of coiled coils, where pH values from 4 to 11 exhibit a primarily coiled coil structure. Values were measured after annealing the sample from 90 to 20 °C at a concentration of 100 mM peptide in water with pH adjustment made with HCl or NaOH. p K_a values of acidic and basic amino acids are indicated to show the correlation between the denaturation of the peptide at those values. Additionally, the estimated net charge of the peptide (Z) is plotted to corroborate these locations, where stability changes occur. The gray regime indicates the pH range at which the peptide precipitation occurs.

represents the extent of helicity, while the ellipticity at 204 nm indicates the presence of a two-state system and remains constant across both folded and unfolded states, making it a suitable reference point for structural changes.³⁹

Based on the CD spectra, a primarily helical structure was observed from a pH between 4 and 11. At pHs lower than 6 or greater than 12, a decrease in the ratio of 222 nm to 204 nm was observed, indicating a transition toward a higher proportion of random coils. This structural shift at these pH values is attributed to the partial protonation or deprotonation of acidic and basic amino acid side chains as their pK_a values are approached. For pH values below 4, a transition from primarily coiled coils to primarily random coils was observed, marked by a shift in CD to a single minimum at 200 nm (see Figure S12A,B). Given that the pK_a values of all the acidic amino acids in the sequence are greater than 4, a pH \leq 4 corresponds to the removal of all negative charges and a shift in the net charge from +4 to +28 per coiled coil. Conversely, at pH \geq 12, peptide precipitation was observed, resulting in no clear CD signal (see Figure S12L). In this pH range, all of the positive charges associated with the basic amino acids are expected to be removed, resulting in a decrease in net charge from +4 to -24 per coiled coil. The shifts in charge from extreme pH adjustment resulted in destabilization of the coiled coil structure, possibly by eliminating stabilizing salt bridge interactions and introducing unfavorable like-charge interactions along the exterior of the coiled coil.

The pH stability of BNDL22 across the pK_a values of the acidic and basic amino acids underscores the robustness of the design centered on the conserved A, I, and M amino acids within the heptad repeat. On the one hand, its stability over a broad range of solution conditions indicates its potential for applications beyond typical biological conditions. On the other hand, the predictable impact of pH on stability provides another dimension to using the coiled coil to design responsive materials. Overall, the robust design and dynamic range of BNDL22 can be used as a responsive building block for a wide range of applications.

BNDL22 Cross-Linked Hydrogels. The BNDL22 coiled coil is both pH- and temperature-responsive under moderate conditions, making it ideal as an adaptive hydrogel cross-linker. Tirrell and co-workers first demonstrated the use of coiled coils in hydrogels, where they designed and created protein-based polyelectrolyte hydrogels that included the leucine zipper coiled coil sequence.8 They demonstrated that physical crosslinking in these hydrogels responded to variations in both pH and temperature. Moreover, BNDL29 has previously been employed as a physical cross-linker in a hydrogel, albeit with limited thermal-responsiveness due to the remarkable thermal stability of BNDL29.1 To use BNDL22 as a tunable dynamic individual cross-linker in a hydrogel, we cross-linked a tetrafunctional PEG-thiol with an allyl-functionalized BNDL22 using a photoinitiated thiol-ene reaction, as shown in Figure 5C. The modified peptide retained is a coiled coil structure under aqueous conditions (Figure S13), resulting in a tetrafunctional cross-linker (see Figure 5).

The dynamic properties of the hydrogel cross-linked BNDL22 were evaluated using oscillatory shear rheometry. The ability to adjust the temperature to denature the BNDL22 cross-linker was expected to induce a solid-like to liquid-like state at elevated temperatures. To demonstrate this, the hydrogel was subjected to heating and cooling cycles, from temperatures above the $T_{\rm m}$ of BNDL22 down to room

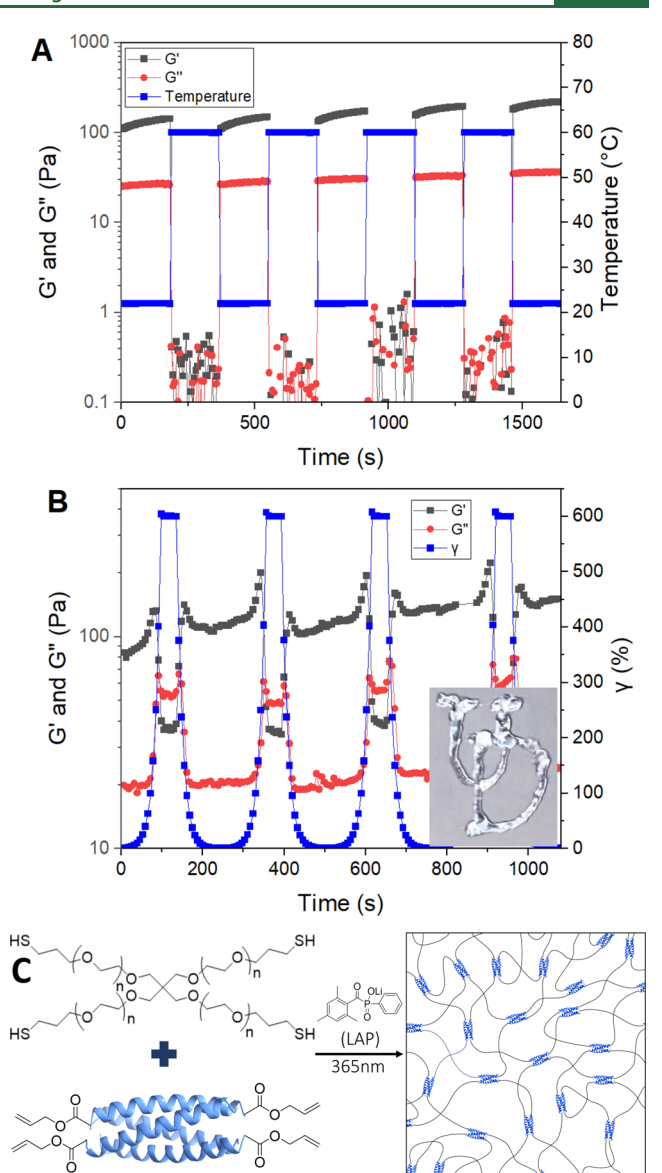


Figure 5. Hydrogel rheometry shows recovery after deformation of BNDL22 cross-linked PEG hydrogels as a function of changes in temperature (A) and strain (B) over time. (A) At high temperature (60 °C), degelation results in hydrogel "melting" into a liquid-like fluid, while at lower temperature (22.5 °C), the hydrogel is reformed as seen in the recovery of G'. (B) Hydrogel shear-induced "melting" at high strain, indicated by the crossover of G' and G''. Inlaid is a gel printed into shape through a needle from a syringe, demonstrating the shear thinning properties allowing for injection. (C) Reaction between tetrafunctional PEG-SH and alloc-modified BNDL22, leading to the formation of a hydrogel.

temperature (see Figure 5A). At room temperature, the hydrogel exhibited a storage modulus (G') greater than the loss modulus (G''), as expected for a solid-like material. When the temperature of the hydrogel was heated to 60 °C, a sol—gel transition was observed, which we demarcate as the crossover of G' and G'' (typically in the vicinity of the actual Winter—Chambon determined gel point). The hydrogel was found to recover over multiple cycles with the modulus returning to approximately the same value, exhibiting a slight increase over time attributed to evaporation. Additionally, the ability to recover the hydrogel properties after heating provides a means for recycling or reprocessing the hydrogel.

The BNDL22 hydrogel, which forms through a physical, coiled coil cross-linking mechanism, was expected to have mechanical properties that respond to any stimuli that induce coiled coil denaturation. Similar responsiveness has been observed in other peptide-based hydrogels, such as the shear thinning behavior of hydrogels formed through the selfassembly of β -hairpin peptides. ⁴¹ The shear-induced reversible cross-linking of the BNDL22 hydrogels was investigated upon the application of large amplitude oscillatory shear. A strain amplitude sweep revealed that the hydrogel exhibited a linear response up to approximately 60% strain (at a frequency of 0.1 Hz) and underwent a sol-gel transition at approximately 500% strain (Figure S14). The reversibility of the strain-induced solgel transition was examined by cycling the strain from 600 to 1%, as shown in Figure 5B. The modulus was recovered after each cycle, indicating that the strain-induced degelation was reversible, which is attributed to the BNDL22 cross-links being physically disrupted and reformed.

Introducing dynamic and tunable stability offers significant advantages for bulk material applications, especially when reversible denaturation is desirable, such as cross-linking a hydrogel. One such scenario where reversible denaturation proves advantageous is for the injection of hydrogels post polymerization, circumventing the need for environmental triggers for polymerization, which can be complex in biological conditions.⁴² The shear-induced degelation of the BNDL22 cross-linked hydrogel implies its potential for injection through a syringe, allowing applications ranging from injectable hydrogel for drug delivery to 3D printing. As a proof of concept, we "printed" U and D shapes by injecting the BNDL22 hydrogel through a needle and syringe as shown in the Figure 5B inset. Furthermore, the thermal behavior demonstrated in Figure 5A could be leveraged to make materials that are recovered and recycled through thermal cycling.

CONCLUSIONS

A series of coiled coil peptides ranging in length from 22 to 8 amino acids were designed de novo. These sequences were derived from a previously designed 29 amino acid sequence, BNDL29. By shortening the peptide sequence via computational design, tunable properties were introduced into the stability of the coiled coil structure; the reduced stabilities are in contrast to the high thermostability of BNDL29. CD spectroscopy analysis revealed that BNDL22 formed coiled coils with a $T_{\rm m}$ of 58 °C, whereas BNDL15 and BNDL8 did not form coiled coils. This result is consistent with previously reported observations that indicate that a minimum of three heptads, as found in BNDL22, is necessary for coiled coil stability without additional stabilization methods like staples (i.e., chemical cross-links) or salt bridge formation.

This study establishes that design rules regarding minimum length observed in dimeric coiled coils extend to tetrameric coiled coils, offering further insights into the behavior of tetrameric coiled coils. 13,28 Additionally, the stability of BNDL22 in solution was investigated under monovalent salt conditions, revealing that $T_{\rm m}$ can be increased via the addition of salt with trends following the Hoffmeister series. This increased stability is attributed to increased hydrophobic effects and the screening of unfavorable interactions along the coiled coil's exterior. Examination of pH effects on BNDL22 revealed resilience to changes in pH over the range of 4 < pH < 11, until the pH = p K_a of acidic or basic side groups of the

constituent amino acids. Under extreme acidic conditions, a transition from coiled coils to random coils occurred, while under extreme basic conditions, precipitation was observed. This broad range of pH stability highlights the versatile applicability of this sequence beyond biological conditions.

Finally, BNDL22 was employed as a physical cross-linker within a PEG hydrogel, introducing dynamic properties to the bulk material. Shear rheology confirmed degelation of the hydrogel at temperatures above the coiled coil $T_{\rm m}$ and at high strain amplitudes. Due to the ability for this hydrogel to recover after shear, the gel could be injected through a syringe to "print" complex shapes. This shear-induced degelation feature opens possibilities for several applications such as 3D printing and injectable hydrogel drug delivery. Overall, this study demonstrated the robustness of these peptides and their broad suitability to materials applications, even in conditions traditionally considered inhospitable to protein and other biobased building blocks.

ASSOCIATED CONTENT

5 Supporting Information

The Supporting Information is available free of charge at https://pubs.acs.org/doi/10.1021/acs.biomac.4c00355.

Table of additional peptide sequences; table of pH values used in CD; UPLC-MS of peptides; additional circular dichroism of peptides at various concentrations, salt, and pH conditions; hydrogel rheology (PDF)

AUTHOR INFORMATION

Corresponding Authors

Jeffery G. Saven — Department of Chemistry, University of Pennsylvania, Philadelphia, Pennsylvania 19104, United States; ⊚ orcid.org/0000-0001-5027-7241; Email: saven@ sas.upenn.edu

Darrin J. Pochan — Department of Materials Science and Engineering, University of Delaware, Newark, Delaware 19716, United States; orcid.org/0000-0002-0454-2339; Email: pochan@udel.edu

Christopher J. Kloxin — Department of Chemical and Biomolecular Engineering, University of Delaware, Newark, Delaware 19716, United States; Department of Materials Science and Engineering, University of Delaware, Newark, Delaware 19716, United States; orcid.org/0000-0002-1679-0022; Email: cjk@udel.edu

Authors

Joshua E. Meisenhelter — Department of Chemical and Biomolecular Engineering, University of Delaware, Newark, Delaware 19716, United States; orcid.org/0009-0001-6330-0364

Nolan R. Petrich – Department of Chemical and Biomolecular Engineering, University of Delaware, Newark, Delaware 19716, United States

Jacquelyn E. Blum – Department of Chemistry, University of Pennsylvania, Philadelphia, Pennsylvania 19104, United States

Albree R. Weisen – Department of Materials Science and Engineering, University of Delaware, Newark, Delaware 19716, United States

Rui Guo — Department of Chemistry, University of Pennsylvania, Philadelphia, Pennsylvania 19104, United States

Complete contact information is available at: https://pubs.acs.org/10.1021/acs.biomac.4c00355

Author Contributions

The manuscript was written through contributions of all authors. All authors have given approval to the final version of the manuscript.

Notes

The authors declare no competing financial interest.

ACKNOWLEDGMENTS

This research was primarily supported by NSF through the University of Delaware Materials Research Science and Engineering Center (MRSEC), Center for Hybrid, Active, and Responsive Materials (CHARM), DMR-2011824 as well as partial support through CHE-2003897. In addition, both the NMR and mass spectrometry facilities at the University of Delaware were supported by the Center for Hybrid, Active, and Responsive Materials (CHARM) and Centers of Biomedical Research Excellence (COBRE) programs through NSF DMR-2011824 and NIH NIGMS-P20GM104316, respectively. Additional support for this work was provided by the Department of Energy (DOE) Office of Basic Energy Sciences, Biomolecular Materials Program under grant nos. DE-SC0019355 and DE-SC0019282. Computational studies were performed using allocation TG-CHE110041 from the Advanced Cyberinfrastructure Coordination Ecosystem: Services & Support (ACCESS) program, which is supported by National Science Foundation grants #1548562, #2138259, #2138286, #2138307, #2137603, and #2138296.

ABBREVIATIONS

alloc, alloxycarbonyl; CD, circular dichroism; TFA, trifluoroacetic acid; $T_{\rm m}$, melting temperature

REFERENCES

- (1) Wu, D.; Sinha, N.; Lee, J.; Sutherland, B. P.; Halaszynski, N. I.; Tian, Y.; Caplan, J.; Zhang, H. V.; Saven, J. G.; Kloxin, C. J.; Pochan, D. J. Polymers with Controlled Assembly and Rigidity Made with Click-Functional Peptide Bundles. *Nature* **2019**, *574* (7780), 658–662.
- (2) Zhang, H. V.; Polzer, F.; Haider, M. J.; Tian, Y.; Villegas, J. A.; Kiick, K. L.; Pochan, D. J.; Saven, J. G. Computationally Designed Peptides for Self-Assembly of Nanostructured Lattices. *Sci. Adv.* **2016**, 2 (9), No. e1600307.
- (3) Bunick, C. G.; Milstone, L. M. The X-Ray Crystal Structure of the Keratin 1-Keratin 10 Helix 2B Heterodimer Reveals Molecular Surface Properties and Biochemical Insights into Human Skin Disease. *J. Invest. Dermatol.* **2017**, *137* (1), 142–150.
- (4) Russell, R. J.; Kerry, P. S.; Stevens, D. J.; Steinhauer, D. A.; Martin, S. R.; Gamblin, S. J.; Skehel, J. J. Structure of Influenza Hemagglutinin in Complex with an Inhibitor of Membrane Fusion. *Proc. Natl. Acad. Sci. U. S. A.* **2008**, *105* (46), 17736–17741.
- (5) Wilson, I. A.; Skehel, J. J.; Wiley, D. C. Structure of the Haemagglutinin Membrane Glycoprotein of Influenza Virus at 3 Å Resolution. *Nature* **1981**, 289 (5796), 366–373.
- (6) Sutton, R. B.; Fasshauer, D.; Jahn, R.; Brunger, A. T. Crystal Structure of a SNARE Complex Involved in Synaptic Exocytosis at 2.4 Å Resolution. *Nature* **1998**, 395 (6700), 347–353.
- (7) Guo, R.; Sinha, N. J.; Misra, R.; Tang, Y.; Langenstein, M.; Kim, K.; Fagan, J. A.; Kloxin, C. J.; Jensen, G.; Pochan, D. J.; Saven, J. G. Computational Design of Homotetrameric Peptide Bundle Variants Spanning a Wide Range of Charge States. *Biomacromolecules* **2022**, 23 (4), 1652–1661.

- (8) Petka, W. A.; Harden, J. L.; McGrath, K. P.; Wirtz, D.; Tirrell, D. A. Reversible Hydrogels from Self-Assembling Artificial Proteins. *Science* **1998**, 281 (5375), 389–392.
- (9) Woolfson, D. N. The Design of Coiled-Coil Structures and Assemblies. In *Advances in Protein Chemistry; Fibrous Proteins: Coiled-Coils, Collagen and Elastomers*; Academic Press, 2005; Vol. 70, pp 79–112. DOI: DOI: 10.1016/S0065-3233(05)70004-8.
- (10) Haider, M. J.; Zhang, H. V.; Sinha, N.; Fagan, J. A.; Kiick, K. L.; Saven, J. G.; Pochan, D. J. Self-Assembly and Soluble Aggregate Behavior of Computationally Designed Coiled-Coil Peptide Bundles. *Soft Matter* **2018**, *14* (26), 5488–5496.
- (11) Kwok, S. C.; Hodges, R. S. Effect of Chain Length on Coiled-Coil Stability: Decreasing Stability with Increasing Chain Length. *Pept. Sci.* **2004**, *76* (5), 378–390.
- (12) Su, J. Y.; Hodges, R. S.; Kay, C. M. Effect of Chain Length on the Formation and Stability of Synthetic.Alpha.-Helical Coiled Coils. *Biochemistry* **1994**, 33 (51), 15501–15510.
- (13) Lau, S. Y.; Taneja, A. K.; Hodges, R. S. Synthesis of a Model Protein of Defined Secondary and Quaternary Structure. Effect of Chain Length on the Stabilization and Formation of Two-Stranded Alpha-Helical Coiled-Coils. *J. Biol. Chem.* 1984, 259 (21), 13253—13261
- (14) Jo, H.; Meinhardt, N.; Wu, Y.; Kulkarni, S.; Hu, X.; Low, K. E.; Davies, P. L.; DeGrado, W. F.; Greenbaum, D. C. Development of α -Helical Calpain Probes by Mimicking a Natural Protein–Protein Interaction. *J. Am. Chem. Soc.* **2012**, *134* (42), 17704–17713.
- (15) Wuo, M. G.; Mahon, A. B.; Arora, P. S. An Effective Strategy for Stabilizing Minimal Coiled Coil Mimetics. *J. Am. Chem. Soc.* **2015**, 137 (36), 11618–11621.
- (16) Drobnak, I.; Gradišar, H.; Ljubetič, A.; Merljak, E.; Jerala, R. Modulation of Coiled-Coil Dimer Stability through Surface Residues While Preserving Pairing Specificity. *J. Am. Chem. Soc.* **2017**, *139* (24), 8229–8236.
- (17) Deng, Y.; Liu, J.; Zheng, Q.; Eliezer, D.; Kallenbach, N. R.; Lu, M. Antiparallel Four-Stranded Coiled Coil Specified by a 3–3-1 Hydrophobic Heptad Repeat. *Structure* **2006**, *14* (2), 247–255.
- (18) MacKerell, A. D., Jr.; Bashford, D.; Bellott, M.; Dunbrack, R. L., Jr.; Evanseck, J. D.; Field, M. J.; Fischer, S.; Gao, J.; Guo, H.; Ha, S.; Joseph-McCarthy, D.; Kuchnir, L.; Kuczera, K.; Lau, F. T. K.; Mattos, C.; Michnick, S.; Ngo, T.; Nguyen, D. T.; Prodhom, B.; Reiher, W. E.; Roux, B.; Schlenkrich, M.; Smith, J. C.; Stote, R.; Straub, J.; Watanabe, M.; Wiórkiewicz-Kuczera, J.; Yin, D.; Karplus, M. All-Atom Empirical Potential for Molecular Modeling and Dynamics Studies of Proteins. J. Phys. Chem. B 1998, 102 (18), 3586–3616.
- (19) Chen, V. B.; Arendall, W. B.; Headd, J. J.; Keedy, D. A.; Immormino, R. M.; Kapral, G. J.; Murray, L. W.; Richardson, J. S.; Richardson, D. C. MolProbity: All-Atom Structure Validation for Macromolecular Crystallography. *Acta Crystallogr. D Biol. Crystallogr.* **2010**, *66* (1), 12–21.
- (20) Chan, E. by W, C., White, P. D., Eds.; Fmoc Solid Phase Peptide Synthesis: A Practical Approach; Practical Approach Series; Oxford University Press: Oxford, NY, 2000.
- (21) Coin, I.; Beyermann, M.; Bienert, M. Solid-Phase Peptide Synthesis: From Standard Procedures to the Synthesis of Difficult Sequences. *Nat. Protoc.* **2007**, *2* (12), 3247–3256.
- (22) Ford, E. M.; Kloxin, A. M. Rapid Production of Multifunctional Self-Assembling Peptides for Incorporation and Visualization within Hydrogel Biomaterials. *ACS Biomater. Sci. Eng.* **2021**, *7* (9), 4175–4195.
- (23) Greenfield, N. J. Using Circular Dichroism Spectra to Estimate Protein Secondary Structure. *Nat. Protoc.* **2006**, *1* (6), 2876–2890.
- (24) Sawicki, L. A.; Kloxin, A. M. Design of Thiol–Ene Photoclick Hydrogels Using Facile Techniques for Cell Culture Applications. *Biomater. Sci.* **2014**, 2 (11), 1612–1626.
- (25) Zhou, N. E.; Zhu, B.-Y.; Kay, C. M.; Hodges, R. S. The Two-Stranded α -Helical Coiled-Coil Is an Ideal Model for Studying Protein Stability and Subunit Interactions. *Biopolymers* **1992**, 32 (4), 419–426.

- (26) Zhou, N. E.; Kay, C. M.; Hodges, R. S. Synthetic Model Proteins. Positional Effects of Interchain Hydrophobic Interactions on Stability of Two-Stranded Alpha-Helical Coiled-Coils. *J. Biol. Chem.* **1992**, 267 (4), 2664–2670.
- (27) Greenfield, N. J.; Hitchcock-Degregori, S. E. Conformational Intermediates in the Folding of a Coiled-Coil Model Peptide of the N-Terminus of Tropomyosin and A α -Tropomyosin. *Protein Sci.* **1993**, 2 (8), 1263–1273.
- (28) Fairman, R.; Chao, H. G.; Mueller, L.; Lavoie, T. B.; Shen, L.; Novotny, J.; Matsueda, G. R. Characterization of a New Four-Chain Coiled-Coil: Influence of Chain Length on Stability. *Protein Sci. Publ. Protein Soc.* 1995, 4 (8), 1457–1469.
- (29) Kang, B.; Tang, H.; Zhao, Z.; Song, S. Hofmeister Series: Insights of Ion Specificity from Amphiphilic Assembly and Interface Property. ACS Omega 2020, 5 (12), 6229–6239.
- (30) Crevenna, A. H.; Naredi-Rainer, N.; Lamb, D. C.; Wedlich-Söldner, R.; Dzubiella, J. Effects of Hofmeister Ions on the α -Helical Structure of Proteins. *Biophys. J.* **2012**, *102* (4), 907–915.
- (31) Arakawa, T.; Timasheff, S. N. Preferential Interactions of Proteins with Salts in Concentrated Solutions. *Biochemistry* **1982**, 21 (25), 6545–6552.
- (32) Kohn, W. D.; Kay, C. M.; Hodges, R. S. Salt Effects on Protein Stability: Two-Stranded α -Helical Coiled-Coils Containing Inter- or Intrahelical Ion pairs11Edited by P. E. Wright. *J. Mol. Biol.* **1997**, 267 (4), 1039–1052.
- (33) Li, X.; Fei, S.; Xie, X.; Tong, P.; Yuan, J.; Wu, Z.; Yang, A.; Wu, Y.; Chen, H. Effects of Divalent Cations on the Physical, Conformational and Immunological Properties of Bovine Allergen β -Lactoglobulin Aggregates. *LWT* **2022**, *154*, No. 112557.
- (34) Arakawa, T.; Timasheff, S. N. Mechanism of Protein Salting in and Salting out by Divalent Cation Salts: Balance between Hydration and Salt Binding. *Biochemistry* **1984**, *23* (25), 5912–5923.
- (35) Okur, H. I.; Hladílková, J.; Rembert, K. B.; Cho, Y.; Heyda, J.; Dzubiella, J.; Cremer, P. S.; Jungwirth, P. Beyond the Hofmeister Series: Ion-Specific Effects on Proteins and Their Biological Functions. *J. Phys. Chem. B* **2017**, *121* (9), 1997–2014.
- (36) Hofmeister, F. Zur Lehre von der Wirkung der Salze. Arch. Für Exp. Pathol. Pharmakol. 1888, 24 (4), 247–260.
- (37) Dutta, K.; Alexandrov, A.; Huang, H.; Pascal, S. M. pH-Induced Folding of an Apoptotic Coiled Coil. *Protein Sci. Publ. Protein Soc.* **2001**, *10* (12), 2531–2540.
- (38) Yu, Y.; Monera, O. D.; Hodges, R. S.; Privalov, P. L. Ion Pairs Significantly Stabilize Coiled-Coils in the Absence of Electrolyte. *J. Mol. Biol.* **1996**, 255 (3), 367–372.
- (39) Holtzer, M. E.; Holtzer, A. α -Helix to Random Coil Transitions: Determination of Peptide Concentration from the CD at the Isodichroic Point. *Biopolymers* **1992**, 32 (12), 1675–1677.
- (40) Winter, H. H. Can the Gel Point of a Cross-Linking Polymer Be Detected by the G' G" Crossover? *Polym. Eng. Sci.* **1987**, 27 (22), 1698–1702.
- (41) Haines-Butterick, L.; Rajagopal, K.; Branco, M.; Salick, D.; Rughani, R.; Pilarz, M.; Lamm, M. S.; Pochan, D. J.; Schneider, J. P. Controlling Hydrogelation Kinetics by Peptide Design for Three-Dimensional Encapsulation and Injectable Delivery of Cells. *Proc. Natl. Acad. Sci. U. S. A.* **2007**, *104* (19), 7791–7796.
- (42) Correa, S.; Grosskopf, A. K.; Lopez Hernandez, H.; Chan, D.; Yu, A. C.; Stapleton, L. M.; Appel, E. A. Translational Applications of Hydrogels. *Chem. Rev.* **2021**, *121* (18), 11385–11457.